POLITECNICO DI TORINO
Repository ISTITUZIONALE

Shell finite elements with different through-the-thickness kinematics for the linear analysis of cylindrical multilayered structures.

(Article begins on next page)

19 April 2024

Shell finite elements with different through-the-thickness kinematics for the linear analysis of cylindrical multilayered structures

M. Cinefra[*,†] and E. Carrera

Aerospace Department, Politecnico di Torino, Corso Duca degli Abruzzi, 24, 10129 Turin, Italy

SUMMARY

The present paper considers the linear static analysis of composite cylindrical structures by means of a shell finite element with variable through-the-thickness kinematic. The refined models used are grouped in the Unified Formulation by Carrera (CUF), and they permit to accurately describe the distribution of displacements and stresses along the thickness of the multilayered shell. The shell element has nine nodes, and the mixed interpolation of tensorial components method is employed to contrast the membrane and shear locking phenomenon. Different composite cylindrical shells are analyzed, with various laminations and thickness ratios. The governing equations are derived from the principle of virtual displacement in order to apply the finite element method. The results, obtained with different theories contained in the CUF, are compared with both the elasticity solutions given in the literature and the analytical solutions obtained using Navier's method. From the analysis, one can conclude that the shell element based on the CUF is very efficient, and its use is mandatory with respect to the classical models in the study of composite structures. Copyright © 2012 John Wiley & Sons, Ltd.

1. INTRODUCTION

Layered structures are increasingly used in aerospace, automotive, and ship vehicles. The so-called advanced composite materials were developed as part of aerospace vehicles during the second part of the last century. Nowadays, there are examples of fighter and commercial aircrafts, helicopters, and gliders whose structures are entirely made of composite materials. A more recent example of layered structures is that of intelligent structures that embed piezo-layers and which are used as sensors and/or actuators to build a closed-loop controlled 'smart' structure.

Anisotropy, nonlinear analysis as well as complicating effects such as the C_z^0-Requirements (zigzag effects in the displacements and interlaminar continuity for the stresses), and the couplings between in-plane and out-of-plane strains make the analysis of layered composite structures complicated in practice. Analytical, closed-form solutions are available in very few cases. In most of the practical problems, the solutions demand applications of approximated computational methods.

Many computational techniques have been developed and applied to layered constructions. A full mixed 3D finite difference technique was developed by Noor and Rarig [1]. More recently, a differential quadrature technique has been proposed by Malik [2] and Malik and Bert [3] and applied by Liew *et al*. [4]. A boundary element formulation has been employed by Davì in [5].

---

*Correspondence to: M. Cinefra, Aerospace Department, Politecnico di Torino, Corso Duca degli Abruzzi, 24, 10129 Turin, Italy.

†E-mail: maria.cinefra@polito.it

Ferreira *et al*. [6–8] adopt a meshless collocation method based on the use of radial basis functions for the analysis of laminated plates and shells. Exhaustive overviews on several computational techniques and their applications to laminated structures can be read in the review articles [9–11].

Among the computational techniques implemented for the analysis of layered structures, a predominant role has been played by finite element method (FEM). The most of finite elements available in the literature are formulated on the bases of axiomatic-type theories, in which the unknown variables are postulated along the thickness. According to MacNeal [12], the first FEM analysis was published in 1961. The majority of early FEM calculations were performed with the classical Kirchhoff–Love theory, and some examples are given in [13–17]. But it was difficult to satisfy the requirements of compatibility in thin shell analysis because the rotations were derived from the transversal displacement. For this reason, plate/shell elements based on the first-order shear deformation theory (FSDT) were developed by Pryor and Barker [18], Noor [19], Hughes [20], Panda and Natarayan [21], Parisch [22], Ferreira *et al*. [23], and many others. However, early FSDT-type elements showed severe stiffening in thin plate/shell limits. Such a numerical mechanism, known as shear or membrane locking, was first contrasted by implementation of numerical tricks, such as reduced/selective integration schemes [24–28]. But spurious zero energy modes are introduced by these sub-integration techniques. Chinosi *et al*. [29, 30] developed a hierarchic finite element for thin Naghdi shell model [31] that was able to contrast locking for the shell problem in its displacement formulation. However, in the case of very small thickness and when the element is not of degree as high as needed, the numerical solution exhibits a loss in the rate of convergence because of the locking. The so-called mixed interpolation of tensorial components (MITC) was implemented to overcome both these problems. Many articles by Bathe and others are available on that topic: examples are the papers [32–37]. Arnold and Brezzi [38] dealt with a mixed formulation of the Nagdi model, giving a family of locking-free elements and proving the convergence of their numerical approach. Similarly, Ramm and Bischoff [39–43] developed a shell finite element based on a seven-parameter theory, in which the extra strain term is incorporated via the enhanced assumed strain concept proposed by Simo and Rafai [44].

Also, a large variety of plate/shell finite element implementations of higher-order theories (HOT) have been proposed in the last 20 years' literature. HOT-based C^0 finite elements (C^0 means that the continuity is required only for the unknown variables and not for their derivatives) were discussed by Kant and co-authors [45, 46]. Polit *et al*. [47–51] proposed a C^1 six-node triangular finite element in which the transverse shear strains are represented by cosine functions. This element is able to ensure both the continuity conditions for displacements and transverse shear stresses at the interfaces between layers of laminated structures. A comprehensive discussion of HOT-type theories and related finite element suitability has been provided by Tessler [52]. Many other papers are available in which HOTs have been implemented for plates and shells; details can be found in the books by Reddy [53] and Palazotto and Dennis [54].

Dozens of finite elements have been proposed based on zigzag theories [55, 56]. An application of Reissner mixed variational theorem (RMVT) [57] to develop standard finite elements was proposed by Rao and Meyer-Piening [58]. A generalization of RMVT as a tool to develop approximate solutions was given by Carrera [59]. The obtained finite elements represent the finite element implementation of the Murakami theory [60] and were denoted by the acronym RMZC (Reissner Mindlin zigzag interlaminar continuity). Full extensions of RMZC to shell geometries have been done by Brank and Carrera [61]. Finally, finite element implementations of layer-wise theories in the framework of axiomatic-type theories have been proposed by many authors, among whom are Noor and Burton [62], Reddy [63], Mawenya and Davies [64], Pinsky and Kim [65], Chaudhuri and Seide [66], and Rammerstorfer *et al*. [67].

An improved shell finite element is here presented for the analysis of composite structures. It is based on Carrera's Unified Formulation (CUF), which was developed by Carrera for multilayered structures [68, 69]. Both equivalent single layer (ESL) and layer-wise (LW) theories contained in the CUF have been implemented in the shell finite element. The cylindrical geometry is considered, and the MITC method [70–73] is used to contrast the membrane and shear locking. The governing equations for the static analysis of composite structures are derived from the principle of virtual displacement (PVD) in order to apply the FEM. Some composite cylindrical shells are analyzed,

and the results obtained with the different models contained in the CUF are compared with the exact solution given in the literature.

2. UNIFIED FORMULATION

The main feature of the CUF [59] is the unified manner in which the displacement variables are handled. According to the CUF, the displacement field is written by means of approximating functions in the thickness direction as follows:

$$\delta \boldsymbol{u}^k \left(\xi_1, \xi_2, \xi_3\right) = F_\tau \left(\xi_3\right) \delta \boldsymbol{u}^k_\tau \left(\xi_1, \xi_2\right); \quad \boldsymbol{u}^k \left(\xi_1, \xi_2, \xi_3\right) = F_s \left(\xi_3\right) \boldsymbol{u}^k_s \left(\xi_1, \xi_2\right) \quad \tau, s = 0, 1, \ldots, N \tag{1}$$

where (ξ_1, ξ_2, ξ_3) is a curvilinear reference system, defined in the next section, and the displacement $\boldsymbol{u} = \{u, v, w\}$ is referred to such system. $\delta \boldsymbol{u}$ indicates the virtual displacement associate with the virtual work, and k identifies the layer. F_τ and F_s are the so-called thickness functions depending only on ξ_3. $\boldsymbol{u}_s$ are the unknown variables depending on the coordinates ξ_1 and ξ_2. τ and s are sum indexes, and N is the order of expansion in the thickness direction assumed for the displacements.

In the case of ESL models, a Taylor expansion is employed as thickness functions:

$$\boldsymbol{u} = F_0 \, \boldsymbol{u}_0 + F_1 \, \boldsymbol{u}_1 + \ldots + F_N \, \boldsymbol{u}_N = F_s \, \boldsymbol{u}_s, \qquad s = 0, 1, \ldots, N. \tag{2}$$

$$F_0 = \xi_3^0 = 1, \quad F_1 = \xi_3^1 = \xi_3, \ldots, F_N = \xi_3^N. \tag{3}$$

Classical models, such as those based on the FSDT [31], can be obtained from an ESL theory with $N = 1$ by imposing a constant transverse displacement through the thickness via penalty techniques. Also, a model based on the hypotheses of classical lamination theory (CLT) [74, 75] can be expressed by means of the CUF by applying a penalty technique to the constitutive equations (Section 4). This permits to impose that the transverse shear strains are null in the shell.

In the case of LW models, the displacement is defined at k-layer level:

$$\boldsymbol{u}^k = F_t \, \boldsymbol{u}^k_t + F_b \, \boldsymbol{u}^k_b + F_r \, \boldsymbol{u}^k_r = F_s \, \boldsymbol{u}^k_s, \qquad s = t, b, r, \qquad r = 2, \ldots, N. \tag{4}$$

$$F_t = \frac{P_0 + P_1}{2}, \quad F_b = \frac{P_0 - P_1}{2}, \quad F_r = P_r - P_{r-2}, \tag{5}$$

in which $P_j = P_j(\zeta_k)$ is the Legendre polynomial of j-order defined in the ζ_k-domain: $-1 \leq \zeta_k \leq 1$. The top (t) and bottom (b) values of the displacements are used as unknown variables, and one can impose the following compatibility conditions:

$$u^k_t = u^{k+1}_b, \qquad k = 1, N_l - 1. \tag{6}$$

The LW models, in respect to the ESLs, allow the zigzag form of the displacement distribution in layered structures to be modeled. It is possible to reproduce the zigzag effects also in the framework of the ESL description by employing the Murakami theory. According to reference [60], a zigzag term can be introduced into Equation (7) as follows:

$$\boldsymbol{u}^k = F_0 \, \boldsymbol{u}^k_0 + \ldots + F_N \, \boldsymbol{u}^k_N + (-1)^k \zeta_k \boldsymbol{u}^k_Z. \tag{7}$$

Subscript Z refers to the introduced term. Such theories are called zigzag (ZZ) theories.

3. MITC9 SHELL ELEMENT

In this section, the derivation of a shell finite element for the analysis of multilayered structures is presented. The element is based on the ESL, ZZ, and LW theories contained in the CUF. A nine-node element with cylindrical geometry is considered. After an overview in the scientific literature about the methods that permit to withstand the membrane and shear locking, the MITC technique has been adopted for this element.
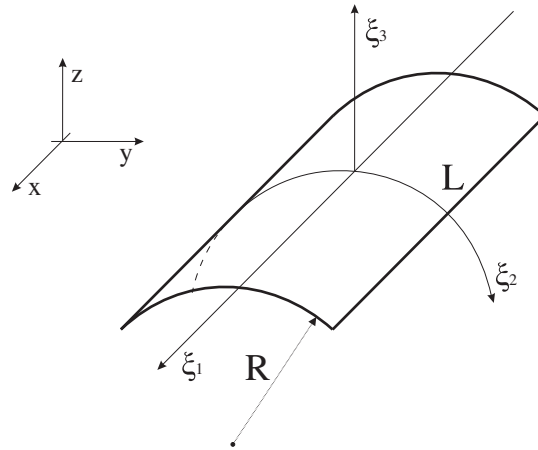
Figure 1. Geometry of the shell.

3.1. Cylindrical geometry

Let us consider a cylindrical shell. In a system of Cartesian coordinates (O, x, y, z), the region occupied by the midsurface of the shell is as follows:

$$S = \left\{ (x, y, z) \in R^3 : \; -L/2 < x < L/2, \; y^2 + z^2 = R^2 \right\} \tag{8}$$

where L and R are the length and the curvature radius of the cylindrical shell, respectively. Let us take a curvilinear coordinate system (ξ_1, ξ_2, ξ_3) placed at the center of the upper part of the midsurface (Figure 1). The 3D medium corresponding to the shell is defined by the 3D chart given by the following:

$$\mathbf{\Phi}(\xi_1, \xi_2, \xi_3) = \boldsymbol{\phi}(\xi_1, \xi_2) + \xi_3 \boldsymbol{a}_3(\xi_1, \xi_2) \tag{9}$$

where $\boldsymbol{a}_3$ is the unit vector normal to the tangent plane to the midsurface of the shell. $\boldsymbol{\phi}$ is the 2D chart that describes the midsurface S of the shell, and, in the case of cylindrical geometry, it reads as follows:

$$\begin{cases} x = \phi_1(\xi_1, \xi_2) = \xi_1 \\ y = \phi_2(\xi_1, \xi_2) = R \sin(\xi_2/R) \\ z = \phi_3(\xi_1, \xi_2) = R \cos(\xi_2/R) \end{cases} \tag{10}$$

With such choices, the region $\Omega \subset R^2$ corresponding to the midsurface S is the following rectangle:

$$\Omega = \{(\xi_1, \xi_2) : \; -L/2 < \xi_1 < L/2, \; -R\pi < \xi_2 < R\pi\} \tag{11}$$

Using the definition of the 3D chart given in (9), one can derive the 3D base vectors:

$$\boldsymbol{g}_\alpha = \frac{\partial \mathbf{\Phi}}{\partial \xi_\alpha}, \qquad \alpha = 1, 2, 3. \tag{12}$$

In order to derive the geometrical relations, one can use the linear part of the Green–Lagrange strain tensor, which for a general displacement $\boldsymbol{u}(\xi_1, \xi_2, \xi_3)$ is as follows:

$$\boldsymbol{\varepsilon}_{ij} = \frac{1}{2} \left(\boldsymbol{g}_i \cdot \boldsymbol{u},_j + \boldsymbol{g}_j \cdot \boldsymbol{u},_i \right), \qquad i, j = 1, 2, 3. \tag{13}$$

where the comma indicates a partial differentiation. According to Equation (12) and the CUF (1), one can write the following strain–displacement relations:

$$
\begin{aligned}
\varepsilon_{11} &= F_\tau u_{\tau,1} \\
\varepsilon_{22} &= F_\tau \left[\left(1 + \frac{\xi_3}{R} \right) \frac{w_\tau}{R} + \left(1 + \frac{\xi_3}{R} \right) v_{\tau,2} \right] \\
\varepsilon_{12} &= F_\tau \left[u_{\tau,2} + \left(1 + \frac{\xi_3}{R} \right) v_{\tau,1} \right] \\
\varepsilon_{13} &= w_{\tau,1} F_\tau + u_\tau F_{\tau,3} \\
\varepsilon_{23} &= F_\tau \left[w_{\tau,2} - \frac{v_\tau}{R} \right] + F_{\tau,3} \left[\left(1 + \frac{\xi_3}{R} \right) v_\tau \right] \\
\varepsilon_{33} &= w_\tau F_{\tau,3}
\end{aligned}
\tag{14}
$$

For more details about mathematical passages, the readers can refer to [76]. These geometrical relations can be expressed in matrix form as follows:

$$
\begin{aligned}
\boldsymbol{\varepsilon}_p &= \left(\boldsymbol{D}_p + \boldsymbol{A}_p \right) \boldsymbol{u} \\
\boldsymbol{\varepsilon}_n &= \left(\boldsymbol{D}_{n\Omega} + \boldsymbol{D}_{nz} - \boldsymbol{A}_n \right) \boldsymbol{u}
\end{aligned}
\tag{15}
$$

where $\boldsymbol{\varepsilon}_p = (\varepsilon_{11}, \varepsilon_{22}, \varepsilon_{12})$ and $\boldsymbol{\varepsilon}_n = (\varepsilon_{13}, \varepsilon_{23}, \varepsilon_{33})$. The differential operators are defined as follows:

$$
\boldsymbol{D}_p = \begin{bmatrix} \partial_1 & 0 & 0 \\ 0 & H\partial_2 & 0 \\ \partial_2 & H\partial_1 & 0 \end{bmatrix}, \quad
\boldsymbol{D}_{n\Omega} = \begin{bmatrix} 0 & 0 & \partial_1 \\ 0 & 0 & \partial_2 \\ 0 & 0 & 0 \end{bmatrix}, \quad
\boldsymbol{D}_{nz} = \partial_3 \cdot \boldsymbol{A}_{nz} = \partial_3 \begin{bmatrix} 1 & 0 & 0 \\ 0 & H & 0 \\ 0 & 0 & 1 \end{bmatrix}, \tag{16}
$$

$$
\boldsymbol{A}_p = \begin{bmatrix} 0 & 0 & 0 \\ 0 & 0 & \frac{1}{R}H \\ 0 & 0 & 0 \end{bmatrix}, \,
\boldsymbol{A}_n = \begin{bmatrix} 0 & 0 & 0 \\ 0 & \frac{1}{R} & 0 \\ 0 & 0 & 0 \end{bmatrix}. \tag{17}
$$

and $H = \left(1 + \frac{\xi_3}{R} \right)$.

3.2. Mixed interpolation of tensorial components method

According to the FEM, the displacement components are interpolated on the nodes of the element by means of the Lagrangian shape functions N_i:

$$
\delta \boldsymbol{u}_\tau = N_i \delta \boldsymbol{q}_{\tau_i} \qquad \boldsymbol{u}_s = N_j \boldsymbol{q}_{s_j} \qquad \text{with} \quad i, j = 1, \dots, 9 \tag{18}
$$

where $\boldsymbol{q}_{s_j}$ and $\delta \boldsymbol{q}_{\tau_i}$ are the nodal displacements and their virtual variations. Substituting in the geometrical relations (15), one has the following:

$$
\begin{aligned}
\boldsymbol{\varepsilon}_p &= F_\tau \left(\boldsymbol{D}_p + \boldsymbol{A}_p \right) \left(N_i \boldsymbol{I} \right) \boldsymbol{q}_{\tau_i} \\
\boldsymbol{\varepsilon}_n &= F_\tau \left(\boldsymbol{D}_{n\Omega} - \boldsymbol{A}_n \right) \left(N_i \boldsymbol{I} \right) \boldsymbol{q}_{\tau_i} + F_{\tau,3} \boldsymbol{A}_{nz} \left(N_i \boldsymbol{I} \right) \boldsymbol{q}_{\tau_i}
\end{aligned}
\tag{19}
$$

where $\boldsymbol{I}$ is the identity matrix.

Considering the local coordinate system (ξ, η), the MITC shell elements ([77, 78]) are formulated by using, instead of the strain components directly computed from the displacements, an interpolation of these within each element using a specific interpolation strategy for each component. The corresponding interpolation points, called tying points, are shown in Figure 2 for a nine-node element. Note that the transverse normal strain ε_{33} is excluded from this procedure, and it is directly calculated from the displacements.
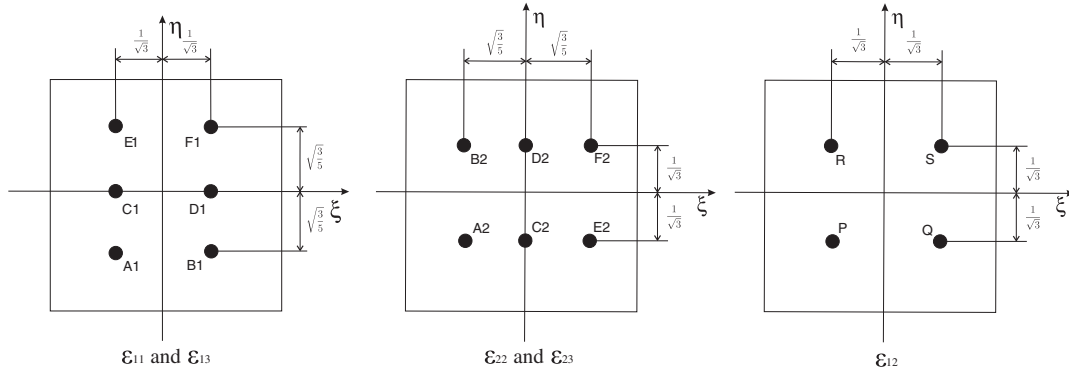
Figure 2. Tying points for the MITC9 shell finite element.

The interpolating functions are calculated by imposing that the function assumes the value 1 in the corresponding tying point and 0 in the others. These are arranged in the following arrays:

$$
\begin{aligned}
N_{m1} &= [N_{A1}, N_{B1}, N_{C1}, N_{D1}, N_{E1}, N_{F1}] \\
N_{m2} &= [N_{A2}, N_{B2}, N_{C2}, N_{D2}, N_{E2}, N_{F2}] \\
N_{m3} &= [N_P, N_Q, N_R, N_S]
\end{aligned}
\tag{20}
$$

From this point on, the subscripts $m1$, $m2$, and $m3$ indicate quantities calculated in the points $(A1, B1, C1, D1, E1, F1)$, $(A2, B2, C2, D2, E2, F2)$, and (P, Q, R, S), respectively. Therefore, the strain components are interpolated as follows:

$$
\begin{aligned}
\boldsymbol{\varepsilon}_p &= \begin{bmatrix} \varepsilon_{11} \\ \varepsilon_{22} \\ \varepsilon_{12} \end{bmatrix} = \begin{bmatrix} N_{m1}\boldsymbol{I} & 0 & 0 \\ 0 & N_{m2}\boldsymbol{I} & 0 \\ 0 & 0 & N_{m3}\boldsymbol{I} \end{bmatrix} \begin{bmatrix} \varepsilon_{11_{m1}} \\ \varepsilon_{22_{m2}} \\ \varepsilon_{12_{m3}} \end{bmatrix} \\
\boldsymbol{\varepsilon}_n &= \begin{bmatrix} \varepsilon_{13} \\ \varepsilon_{23} \\ \varepsilon_{33} \end{bmatrix} = \begin{bmatrix} N_{m1}\boldsymbol{I} & 0 & 0 \\ 0 & N_{m2}\boldsymbol{I} & 0 \\ 0 & 0 & 1 \end{bmatrix} \begin{bmatrix} \varepsilon_{13_{m1}} \\ \varepsilon_{23_{m2}} \\ \varepsilon_{33} \end{bmatrix}
\end{aligned}
\tag{21}
$$

where the strains $\varepsilon_{11_{m1}}$, $\varepsilon_{22_{m2}}$, $\varepsilon_{12_{m3}}$, $\varepsilon_{13_{m1}}$, and $\varepsilon_{23_{m2}}$ are expressed by means of Equation (19) in which the shape functions N_i are calculated in the tying points.

4. CONSTITUTIVE EQUATIONS

The second step towards the governing equations is the definition of the 3D constitutive equations that permit to express the stresses by means of the strains. The generalized Hooke's law is considered by employing a linear constitutive model for infinitesimal deformations. In a composite material, these equations are obtained in material coordinates $(1, 2, 3)$ for each orthotropic layer k and then rotated in the general curvilinear reference system (ξ_1, ξ_2, ξ_3).

Therefore, the stress–strain relations after the rotation are as follows:

$$
\begin{aligned}
\boldsymbol{\sigma}_p^k &= \boldsymbol{C}_{pp}^k \, \boldsymbol{\varepsilon}_p^k + \boldsymbol{C}_{pn}^k \, \boldsymbol{\varepsilon}_n^k \\
\boldsymbol{\sigma}_n^k &= \boldsymbol{C}_{np}^k \, \boldsymbol{\varepsilon}_p^k + \boldsymbol{C}_{nn}^k \, \boldsymbol{\varepsilon}_n^k
\end{aligned}
\tag{22}
$$

where

$$
\boldsymbol{C}_{pp}^k = \begin{bmatrix} C_{11}^k & C_{12}^k & C_{16}^k \\ C_{12}^k & C_{22}^k & C_{26}^k \\ C_{16}^k & C_{26}^k & C_{66}^k \end{bmatrix} \qquad \boldsymbol{C}_{pn}^k = \begin{bmatrix} 0 & 0 & C_{13}^k \\ 0 & 0 & C_{23}^k \\ 0 & 0 & C_{36}^k \end{bmatrix}
$$

$$
\boldsymbol{C}_{np}^k = \begin{bmatrix} 0 & 0 & 0 \\ 0 & 0 & 0 \\ C_{13}^k & C_{23}^k & C_{36}^k \end{bmatrix} \qquad \boldsymbol{C}_{nn}^k = \begin{bmatrix} C_{55}^k & C_{45}^k & 0 \\ C_{45}^k & C_{44}^k & 0 \\ 0 & 0 & C_{33}^k \end{bmatrix}
\tag{23}
$$

The material coefficients C_{ij} depend on Young's moduli E_1, E_2, and E_3, the shear moduli G_{12}, G_{13}, and G_{23}, and Poisson moduli ν_{12}, ν_{13}, ν_{23}, ν_{21}, ν_{31}, and ν_{32} that characterize the layer material. The mapping of the material tensor from the midsurface onto an arbitrary point in the shell body is here omitted.

5. GOVERNING EQUATIONS

This section presents the derivation of the governing finite element stiffness matrix based on the PVD in the case of multilayered cylindrical shells subjected to mechanical loads.

The PVD for a multilayered structure reads as follows:

$$
\int_{\Omega_k} \int_{A_k} \left\{ \delta\boldsymbol{\varepsilon}_p^{k\,T} \boldsymbol{\sigma}_p^k + \delta\boldsymbol{\varepsilon}_n^{k\,T} \boldsymbol{\sigma}_n^k \right\} \mathrm{d}\Omega_k \mathrm{d}z = \int_{\Omega_k} \int_{A_k} \delta\boldsymbol{u}^k \boldsymbol{p}^k \, \mathrm{d}\Omega_k \mathrm{d}z
\tag{24}
$$

where Ω_k and A_k are the integration domains in the plane and in the thickness direction. The first member of the equation represents the variation of the internal work, whereas the second member is the external work. $\boldsymbol{p}^k = \boldsymbol{p}^k(\xi_1, \xi_2, \xi_3)$ is the mechanical load applied to the structure at layer level. In order to refer the integration domains to the midsurface of each layer in the curvilinear coordinate system, one has to introduce the parameter H as follows:

$$
\int_{\Omega_k} \int_{A_k} \left\{ \delta\boldsymbol{\varepsilon}_p^{k\,T} \boldsymbol{\sigma}_p^k + \delta\boldsymbol{\varepsilon}_n^{k\,T} \boldsymbol{\sigma}_n^k \right\} H \, \mathrm{d}\Omega_k \mathrm{d}\xi_3^k = \int_{\Omega_k} \int_{A_k} \delta\boldsymbol{u}^k \boldsymbol{p}^k H \, \mathrm{d}\Omega_k \mathrm{d}\xi_3^k
\tag{25}
$$

where $H = \left(1 + \frac{\xi_3^k}{R_k} \right)$. R_k is the curvature radius of the midsurface of the layer k and $-\frac{h^k}{2} < \xi_3^k < \frac{h^k}{2}$, where h^k is the thickness of the kth layer.
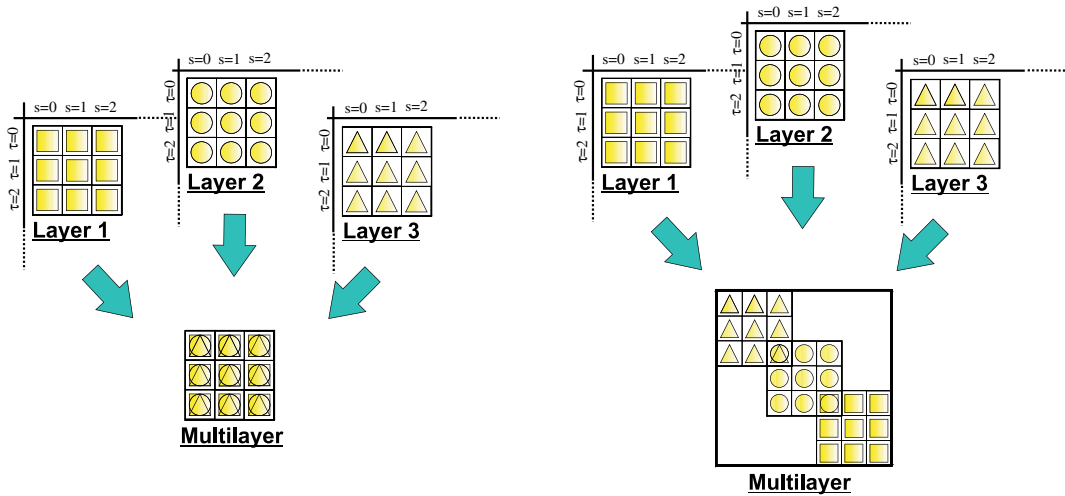

Figure 3. Assembling procedure of fundamental nucleus.

Substituting the constitutive Equation (22) and the geometrical relations written via the MITC method (21) and applying the CUF (1) and the FEM approximation (18), one obtains the following governing equation:

$$\delta \boldsymbol{q}_{\tau_i}^k : \quad \boldsymbol{K}^{k\tau sij} \boldsymbol{q}_{s_j}^k = \boldsymbol{P}_{\tau_i}^k \tag{26}$$

where $\boldsymbol{K}^{k\tau sij}$ is a 3×3 matrix, called fundamental nucleus, and its explicit expression is given in the Appendix. This is the basic element from which the stiffness matrix of the whole structure is computed. The fundamental nucleus is expanded on the indexes τ and s in order to obtain the stiffness matrix of each layer. Then, the matrixes of each layer are assembled at multilayer level depending on the approach considered, ESL or LW. The assembling procedure is shown in Figure 3. $\boldsymbol{P}_{\tau_i}^k$ is the fundamental nucleus for the external mechanical load. For more details, the reader can refer to [68].

6. ACRONYMS

Several refined and advanced 2D models are contained in the CUF. Depending on the variables description (LW, ESL, or ZZ) and the order of expansion N of the displacements in ξ_3, a large variety of kinematics shell theories can be obtained. A system of acronyms is given in order to denote these models. The first letter indicates the multilayer approach which can be ESL (E) or LW (L). The number N indicates the order of expansion used in the thickness direction (from 1 to 4). In the case of LW approach, the same order of expansion is used for each layer. In the case of ESL approach, a letter Z can be added if the zigzag effects of displacements is considered by means of Murakami's zigzag function. Summarizing, E1–E4 are ESL models. If Murakami zigzag function is used, these ESL models are indicated as EZ1–EZ3. In the case of LW approaches, the letter L is considered in place of E, so the acronyms are L1–L4. Classical theories, such as CLT and FSDT, can be obtained as particular cases of E1 theory simply imposing constant value of w through the thickness direction. An appropriate application of penalty technique to shear moduli of the material leads to CLT.

7. NUMERICAL RESULTS AND DISCUSSION

The model introduced, unlike 3D degenerate approach, does not involve an approximation of the geometry of the shell, and it describes accurately the curvature of the shell. However, the locking phenomenon is still present, and the MITC technique is employed to contrast it. In this work, such a model is combined with a simple displacement formulation for the analysis of composite structures. The refined theories contained in the CUF, coupled with the MITC method, permit to increase the degree of approximation by increasing the order of expansion of displacements in the thickness direction and the number of used elements. The efficiency of the different models (ESL, LW, ZZ, and classical) is tested together with the finite element scheme, and the numerical results are compared with the ones obtained with the 3D elasticity approach. In this direction, two classical reference problems are considered: the composite cylindrical shell in cylindrical bending analyzed by Ren [79] and the composite cylinder in bending studied by Varadan and Bhaskar [80]. The two problems are briefly described in the following sections. Note that the problem considered in [79] is denoted as cylindrical bending, although it also exhibits a substantial amount of membrane action.

7.1. Cylindrical shell in cylindrical bending

The structure analyzed by Ren [79] (Figure 4) is a composite cylindrical shell made of three orthotropic layers with lamination $(90°/0°/90°)$, where the lamination angle is measured with respect to the ξ_1 axis. The layers have equal thickness, and the physical properties of the shell are given in Table I (L is the direction parallel to the fibers, and T is the transverse direction).
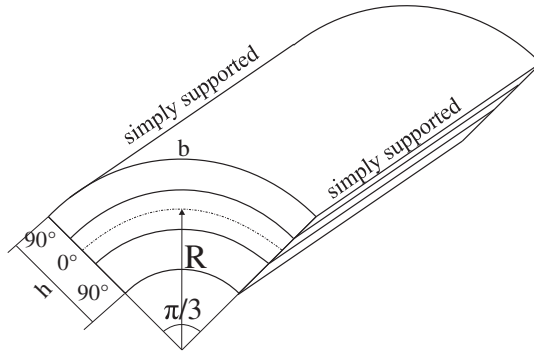
Figure 4. Ren cylindrical shell.

Table I. Physical data for Ren cylindrical shell.

Ren cylindrical shell		
Young's modulus	E_L/E_T	25
Shear modulus	G_{LT}/E_T	0.5
Shear modulus	G_{TT}/E_T	0.2
Poisson's ratio	$\nu_{LT} = \nu_{TT}$	0.25
Radius	R	10
Angle span	φ	$\pi/3$

A sinusoidal distribution of transverse pressure applied at the top shell surface is considered (cylindrical bending problem):

$$p_3^+ = \hat{p}_3^+ \sin\left(\frac{n\,\pi\,\xi_2}{b}\right) \tag{27}$$

with amplitude $\hat{p}_3^+ = 1$ and wave number $n = 1$.

In order to reproduce the property of infinite length in the finite element scheme, the following plane-strain conditions (with respect to the plane ξ_2, ξ_3) are imposed on each point of the cylinder:

$$u_s\,(\xi_1, \xi_2) = 0$$
$$(u_s, v_s, w_s)_{,1}\,(\xi_1, \xi_2) = 0 \tag{28}$$

that is, any variation along the axis of the cylinder is equal to zero.

Because of the symmetry of both the geometry and the load, a half cylinder is taken in the circumferential direction, and the following symmetry and boundary conditions (simply supported) are applied:

$$v_s\,(\xi_1, 0) = 0$$
$$w_s\,(L/2, \xi_2) = 0 \tag{29}$$

with $s = 0, 1, \ldots, N$.

The results are presented for different thickness ratios R/h in terms of non-dimensional transversal displacement:

$$\bar{w} = \frac{w 10 E_L h^3}{\hat{p}_3^+ R^4} \tag{30}$$

measured in the middle of the shell surface, where the load has its maximum amplitude.

Figure 5 shows the convergence of the parameter $\bar{w}$ by varying the number of the elements n in the circumferential direction (only one element is taken in the axial direction) for the theory L4,

and the thickness ratio $R/h = 100$: (MITC) is the FEM solution obtained by applying the MITC method; (FEM$_s$) is the FEM solution with the correction of the shear locking only; and (FEM) is the FEM solution without any correction. One can see that the first curve converges very fast to the 3D solution, as confirmed in Table II, where the percentage error $\left(\text{err} = \frac{|\text{3D}-\text{MITC}|}{\text{3D}} \times 100\right)$ is
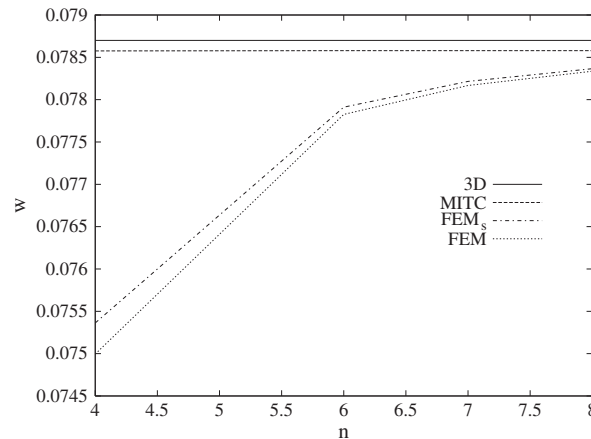

Figure 5. Ren shell. Convergence of the displacement $\bar{w}$ by varying n. Thickness ratio $R/h = 100$. Theory: L4.

Table II. Ren cylindrical shell.

n	2	4	6	8
E4	0.07843	0.07849	0.07850	0.07850
err (%)	0.34	0.27	0.25	0.25
L4	0.07852	0.07857	0.07858	0.07858
err (%)	0.23	0.16	0.15	0.15

Convergence of the transversal displacement $\bar{w}(\xi_3 = 0)$ by increasing the number of elements. Lamination $(90°/0°/90°)$. Thickness ratio $R/h = 100$. Exact solution [79]: 0.0787.
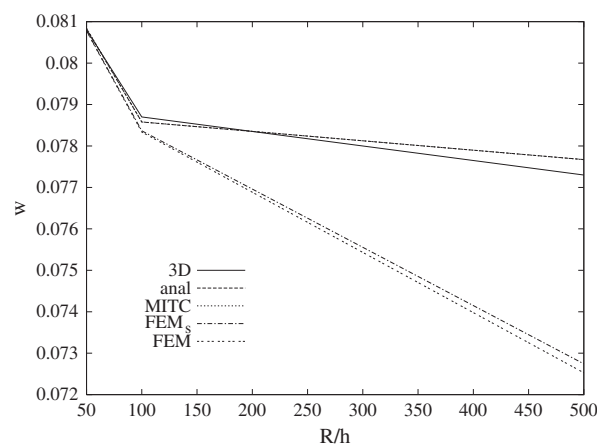

Figure 6. Ren shell. Convergence of the displacement $\bar{w}$ by varying R/h. Theory: L4. Mesh: 1×6.

calculated. One can see that the error becomes steady for $n = 6$, and this fact is true for both ESL (E4) and LW (L4) models. In Figure 5, the other curves are more slow, even when the shear locking is corrected. This demonstrates that the membrane locking is a very important phenomenon in the shell elements, and the MITC technique is very efficient in contrasting both the membrane and shear locking. After this analysis, six elements are taken to perform the following analysis. Finally, Figure 6 shows the convergence of the parameter $\bar{w}$ by varying the thickness ratio R/h for the theory L4. In this figure, the analytical solution (anal), obtained by solving the governing equations with the Navier's method, is also presented for comparison reasons. Navier's method is based on harmonic assumptions for the displacements in the ξ_1 and ξ_2 directions, and it permits to calculate the exact solution in the domain Ω under particular conditions. For more details about this method, one can refer to Reddy's book [53]. One can note that the MITC solution coincides with the analytical one for the different thickness ratios. Therefore, the error of the MITC solution in respect to the exact solution is due only to the bi-dimensional approximation and not to the FEM approximation. This confirms also the efficiency of the MITC method in contrasting the locking, whereas the FEM$_s$ and FEM solutions lock noticeably for very thin shells ($R/h = 100, 500$).

Table III compares the results obtained using the different theories contained in the CUF with the 3D elasticity solution and the classical shell theory (CST) solution given by Ren [79]. For some models (FSDT, E4, E2, L4, L1, EZ2), the analytical solution (a), calculated using Navier's method [81], is also reported. In general, the results approach the exact solution by increasing the order of

Table III. Ren cylindrical shell.

R/h	2	4	50	500
3D [79]	1.436	0.457	0.0808	0.773
CST [79]	0.0799	0.0781	0.0776	0.0776
CLT	0.09625	0.08712	0.07834	0.07766
FSDT	1.169	0.3329	0.07976	0.07766
FSDT$_a$	1.210	0.3354	0.07977	0.07766
E4	1.368	0.4271	0.08051	0.07767
E4$_a$	1.383	0.4284	0.08051	0.07767
E3	1.369	0.4272	0.08051	0.07767
E2	1.104	0.3305	0.07982	0.07766
E2$_a$	1.111	0.3310	0.07982	0.07766
E1	1.129	0.3324	0.07982	0.07766
L4	1.460	0.4614	0.08084	0.07767
L4$_a$	1.435	0.4581	0.08083	0.07767
L3	1.459	0.4614	0.08084	0.07767
L2	1.411	0.4576	0.08083	0.07767
L1	1.381	0.4435	0.08068	0.07764
L1$_a$	1.363	0.4407	0.08067	0.07764
EZ3	1.412	0.4583	0.08084	0.07767
EZ2	1.378	0.4430	0.08071	0.07767
EZ2$_a$	1.496	0.4420	0.08071	0.07767
EZ1	1.400	0.4443	0.08038	0.07734

Lamination ($90°/0°/90°$). Transversal displacement $\bar{w}(\xi_3 = 0)$.

expansion N for the various thickness ratios. For both moderately thick and very thin shells, the solution coincides with the analytical one, and this demonstrates that the element does not suffer the locking or other numerical phenomena. For very low thickness ratio ($R/h = 2, 4$), there are some discrepancies between the two solutions because the 2D approximation is erroneously applied to very thick shells, and the aspect ratio of each element becomes very high. One can note that higher-order zigzag models give a better solution in respect to ESL models, but only the L4 model is able to exactly reproduce the 3D solution in the case of thick shell. This is due to the better approximation of transverse stresses obtained with the LW models, as it will be demonstrated in the following section. Finally, one can conclude that the classical models (FSDT and CLT) give good results only when the shell is very thin ($R/h = 100, 500$). For thick shells, the CLT solution obtained with the CUF shell element is slightly higher than the CST one because the CST model contains more assumptions along the thickness, such as the parameter H (introduced in Equation 25) is equal to 1.

7.2. Composite cylinder in bending

The cylinder analyzed by Varadan and Bhaskar [80] (Figure 7) is a composite cylinder in which each layer is made of square symmetric unidirectional fibrous orthotropic material with the properties given in Table IV. L is the direction parallel to the fibers, and T is the transverse direction.

The following problems are solved:

1. A two-layered ($90°/0°$) shell ($90°$ for the outer layer and $0°$ for the inner layer, measured with respect to the ξ_1 axis);
2. A three-layered ($90°/0°/90°$) shell.

In all these cases, the layers are of equal thickness, and the loading is internal sinusoidal pressure, applied normal to the inner shell surface, and is given by the following:

$$p_3^+ = \hat{p}_3^+ \sin\left(\frac{m \pi \xi_1}{L}\right) \sin\left(\frac{n \pi \xi_2}{b}\right) \tag{31}$$

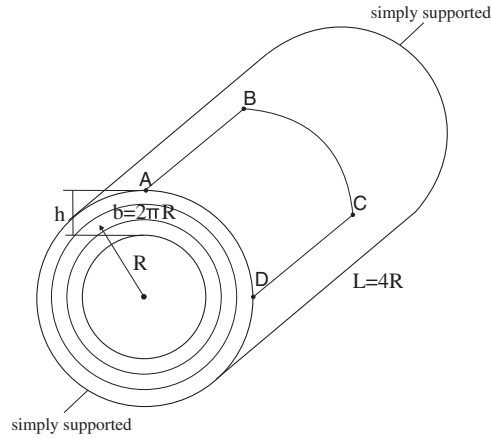with amplitude $\hat{p}_3^+ = 1$ and wave numbers $m = 1$ and $n = 8$.

Figure 7. Varadan and Bhaskar cylinder.

Table IV. Physical data for Varadan and Bhaskar cylinder.

Varadan and Bhaskar cylinder		
Young's modulus	E_L/E_T	25
Shear modulus	G_{LT}/E_T	0.5
Shear modulus	G_{TT}/E_T	0.2
Poisson's ratio	$\nu_{LT} = \nu_{TT}$	0.25
Length	$L = 4R$	40
Radius	R	10

Because of the symmetry of both the geometry and the load, an octave of the cylinder is studied (1/2 in the axial direction and 1/4 in the hoop direction). The following symmetry conditions are applied:

$$v_s\,(\xi_1, 0) = 0$$
$$u_s\,(0, \xi_2) = 0 \tag{32}$$
$$v_s\,(\xi_1, R\pi/2) = 0$$

and the following boundary conditions are prescribed:

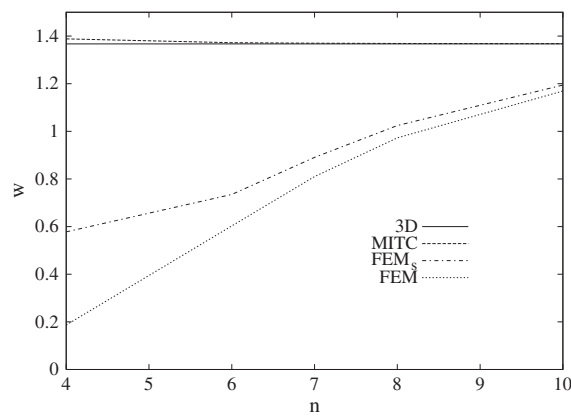$$v_s\,(L/2, \xi_2) = w_s\,(L/2, \xi_2) = 0 \tag{33}$$

with $s = 0, 1, \ldots, N$.

Figure 8. Varadan and Bhaskar cylinder. Convergence of the displacement $\bar{w}$ by varying n. Lamination $(90°/0°)$. Thickness ratio $R/h = 100$. Theory: L4.
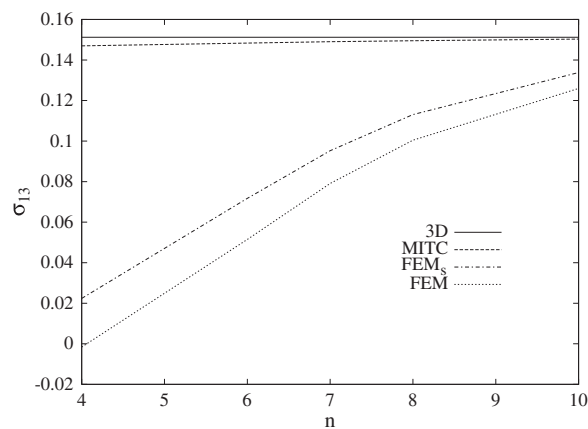

Figure 9. Varadan and Bhaskar cylinder. Convergence of the shear stress $\bar{\sigma}_{13}$ by varying n. Lamination $(90°/0°)$. Thickness ratio $R/h = 100$. Theory: L4.

VARIABLE KINEMATIC MULTILAYERED SHELL ELEMENTS

The results are presented for these cases for different thickness ratios R/h in terms of the following non-dimensional parameters:

$$\bar{w} = \frac{w 10 E_L h^3}{\hat{p}_3^+ R^4}$$

$$(\bar{\sigma}_{11}, \bar{\sigma}_{22}, \bar{\sigma}_{12}) = \frac{(\sigma_{11}, \sigma_{22}, \sigma_{12}) \, 10 h^2}{\hat{p}_3^+ R^2}$$

$$(\bar{\sigma}_{13}, \bar{\sigma}_{23}) = \frac{(\sigma_{13}, \sigma_{23}) \, 10 h}{\hat{p}_3^+ R} \tag{34}$$

$$\bar{\sigma}_{33} = \frac{\sigma_{33}}{\hat{p}_3^+}$$

The displacement and the stresses are evaluated in the points of the surface where they assume the maximum value. Referring to Figure 7, the quantities w, σ_{11}, σ_{22}, and σ_{33} are calculated in B, the shear stress σ_{12} in D, and the transverse shear stresses σ_{13} and σ_{23} in A and C, respectively.

Table V. Varadan and Bhaskar cylinder, transversal displacement.

R/h	2	4	50	500
$\bar{w}(\xi_3 = 0)$ [80]	14.034	6.100	2.242	0.1005
CLT	2.781	2.802	2.227	0.1007
FSDT	12.41	5.578	2.240	0.1007
E4	14.08	6.075	2.242	0.1007
E2	13.07	5.717	2.240	0.1007
L4	14.33	6.164	2.242	0.1007
L2	13.80	5.921	2.241	0.1007
EZ3	14.20	6.009	2.241	0.1007
EZ1	13.67	5.759	2.232	0.1007

Lamination (90°/0°).

Table VI. Varadan and Bhaskar cylinder, in-plane stress.

R/h	2	4	50	500
$\bar{\sigma}_{11}\left(\xi_3 = \mp \frac{h}{2}\right)$ [80]	−2.660	−0.9610	1.610	0.9436
	0.2511	0.2120	0.2189	0.0449
CLT	−0.5690	−0.4752	1.594	0.9484
	0.1464	0.1661	0.2230	0.04535
FSDT	−1.216	−0.6911	1.603	0.9484
	0.2256	0.2018	0.2236	0.04535
E4	−2.649	−0.9580	1.605	0.9486
	0.2302	0.2181	0.2216	0.04516
E2	−2.172	−0.8725	1.606	0.9483
	0.1049	0.1156	0.2226	0.04567
L4	−2.678	−0.9557	1.606	0.9484
	0.2578	0.2210	0.2241	0.04536
L2	−2.610	−0.9386	1.605	0.9484
	0.1986	0.1732	0.2204	0.04534
EZ3	−2.703	−0.9539	1.605	0.9484
	0.2465	0.1970	0.2206	0.04531
EZ1	−1.950	−0.8734	1.567	0.9468
	0.01369	0.1234	0.2483	0.04670

Lamination (90°/0°).

Also in this case, a convergence analysis is performed for the lamination case ($90°/0°$). Figures 8 and 9 show the convergence of the parameters $\bar{w}$ and $\bar{\sigma}_{13}$ by varying the number of the elements n (a square mesh $n \times n$ is used) for the theory L4 and the thickness ratio $R/h = 100$. The conclusions drawn for the Ren shell are here confirmed: the membrane locking is very important for both the displacements and the stresses, and the MITC technique is very efficient in contrasting it. After this analysis, a mesh 8×8 is taken to perform the following analysis.

Tables V–VIII and IX–X show the results for problems 1 and 2, respectively. The different theories contained in the CUF are used, and the results are compared with the 3D solution given in

Table VII. Varadan and Bhaskar cylinder, in-plane shear stress.

R/h	2	4	50	500
$\bar{\sigma}_{12}\left(\xi_3 = \mp\frac{h}{2}\right)$ [80]	−0.5016	−0.2812	−0.3449	−0.1045
	0.2685	0.2007	−0.0784	−0.0925
CLT	−0.1534	−0.1761	−0.3588	−0.1099
	0.1504	0.1516	−0.08235	−0.09736
FSDT	−0.2994	−0.2431	−0.3604	−0.1099
	0.2532	0.1946	−0.08313	−0.09736
E4	−0.4812	−0.2831	−0.3605	−0.1099
	0.3032	0.2199	−0.08280	−0.09736
E2	−0.3677	−0.2521	−0.3602	−0.1099
	0.2541	0.2025	−0.08275	−0.09736
L4	−0.4910	−0.2859	−0.3606	−0.1099
	0.3067	0.2216	−0.08282	−0.09736
L2	−0.4631	−0.2732	−0.3603	−0.1099
	0.2861	0.2103	−0.08276	−0.09736
EZ3	−0.4852	−0.2808	−0.3604	−0.1099
	0.2990	0.2147	−0.08278	−0.09736
EZ1	−0.3636	−0.2553	−0.3589	−0.1099
	0.2715	0.2048	−0.08242	−0.09735

Lamination ($90°/0°$).

Table VIII. Varadan and Bhaskar cylinder, transverse stresses.

R/h	2	4	50	500
$\bar{\sigma}_{23}\left(\xi_3 = \frac{h}{4}\right)$ [80]	−2.931	−4.440	−4.785	−0.227
CLT	–	–	–	–
FSDT	−2.664	−3.216	−2.065	0.3343
E4	−2.928	−4.274	−3.395	0.2764
E2	−2.477	−3.392	−2.386	0.3219
L4	−3.216	−4.791	−5.024	−0.2441
L2	−2.675	−3.671	−3.598	−0.1769
EZ3	−2.971	−3.896	−2.784	0.3019
EZ1	−2.666	−3.494	−2.486	0.3175
$\bar{\sigma}_{33}\left(\xi_3 = \frac{h}{4}\right)$ [80]	−0.31	−0.70	−6.29	−3.09
CLT	–	–	–	–
FSDT	–	–	–	–
E4	−0.3358	−0.7126	−5.072	4.793
E2	−0.3352	−0.6336	−5.197	−12.78
L4	−0.3408	−0.7358	−6.549	−3.082
L2	−0.3440	−0.6612	−4.823	−2.281
EZ3	−0.3353	−0.6899	−4.623	−0.4819
EZ1	−0.3489	−0.6867	−4.927	−2.315

Lamination ($90°/0°$).

VARIABLE KINEMATIC MULTILAYERED SHELL ELEMENTS

Table IX. Varadan and Bhaskar cylinder, transversal
displacement and in-plane stresses.

R/h	2	4	50	500
$\bar{w}(\xi_3 = 0)$ [80]	10.1	4.009	0.5495	0.1027
E4	9.682	3.782	0.5456	0.1029
$E4_a$	9.1582	3.7197	0.5458	0.1027
L4	10.27	4.032	0.5493	0.1029
$L4_a$	10.10	4.009	0.5495	0.1027
$\bar{\sigma}_{11}\left(\xi_3 = \mp\frac{h}{2}\right)$ [80]	−0.8428	−0.2701	−0.0225	0.0379
	0.1761	0.1270	0.0712	0.0559
E4	−0.9447	−0.3011	−0.0240	0.0381
	0.1433	0.1167	0.0730	0.0568
L4	−0.8604	−0.2733	−0.0241	0.0377
	0.1841	0.1330	0.0734	0.0565
$\bar{\sigma}_{12}\left(\xi_3 = \mp\frac{h}{2}\right)$ [80]	−0.2922	−0.1609	−0.0760	−0.0889
	0.1797	0.1081	−0.0118	−0.0766
E4	−0.2770	−0.1568	−0.0791	−0.0935
	0.1957	0.1127	−0.0123	−0.0806
L4	−0.2918	−0.1642	−0.0795	−0.0935
	0.2015	0.1175	−0.0124	−0.0806

Lamination (90°/0°/90°).

Table X. Varadan and Bhaskar cylinder, transverse stresses.

R/h	2	4	50	500
$\bar{\sigma}_{23}(\xi_3 = 0)$ [80]	−1.379	−2.349	−3.491	−0.691
E4	−1.280	−2.025	−2.613	−0.5195
L4	−1.442	−2.464	−3.659	−0.7287
$\bar{\sigma}_{33}(\xi_3 = 0)$ [80]	−0.34	−0.62	−4.85	−9.12
E4	−0.358	−0.684	−5.184	12.26
L4	−0.343	−0.627	−5.026	−9.468

Lamination (90°/0°/90°).

[80]. The analytical solution is also reported for the transversal displacement in problem 2 (Table IX) in order to validate the numerical efficiency of the shell finite element. The results in terms of displacements (Tables V and IX) lead to the same conclusions made for the Ren shell: the results converge to the exact solution by increasing the order of expansion N; the LW models work better than the ESL and ZZ ones; and the CLT and FSDT models fail in the analysis of thick shells. One can note that in problem 1, ESL and ZZ models are better than LW models when the shell is very thick ($R/h = 2$). This is due to the omission of the mapping of the material tensor (Section 4) that causes an overestimate of the transversal displacement when the shell layer is thick. Indeed, when three layers are considered (problem 2), this behavior disappears because each layer is thinner. If one considers the in-plane stresses (Tables VI, VII, and IX), the behavior is the same: higher-order LW models are necessary to match the reference solution in the thick shells, but the classical models are still able to give good results in the thin shell case. Looking at the transverse shear and normal stresses (Tables VIII and X), one can note that neither the E4 and EZ3 models are able to reproduce the exact solution in both thick and thin shells (in particular in terms of σ_{33}). In this case, the use

M. CINEFRA AND E. CARRERA

of the L4 model becomes mandatory. This fact is simply explicable if one considers the distribution of shear and normal stresses along the thickness, given in Figures 10–12. Only the LW model
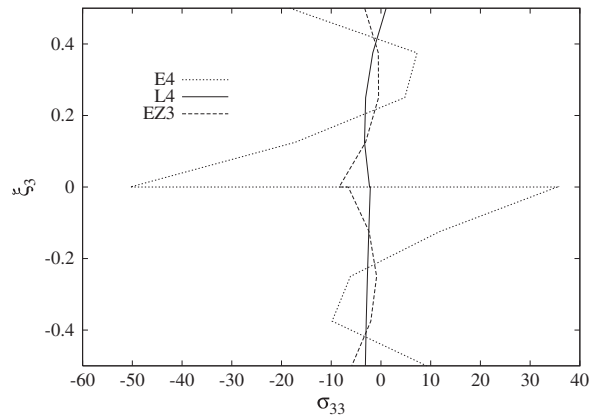
Figure 10. Varadan and Bhaskar cylinder. Distribution of transverse normal stress $\bar{\sigma}_{33}$ along the thickness. Lamination ($90°/0°$). Thickness ratio $R/h = 500$.
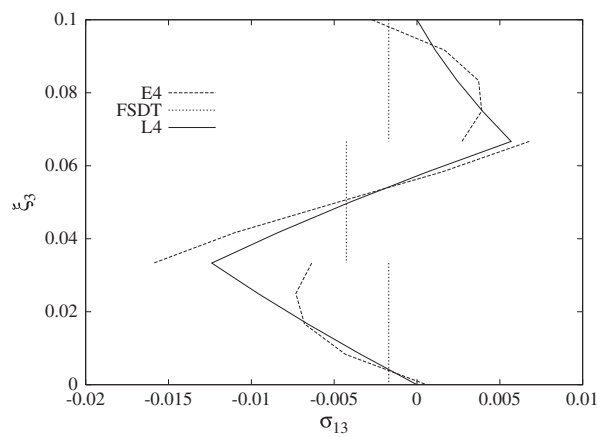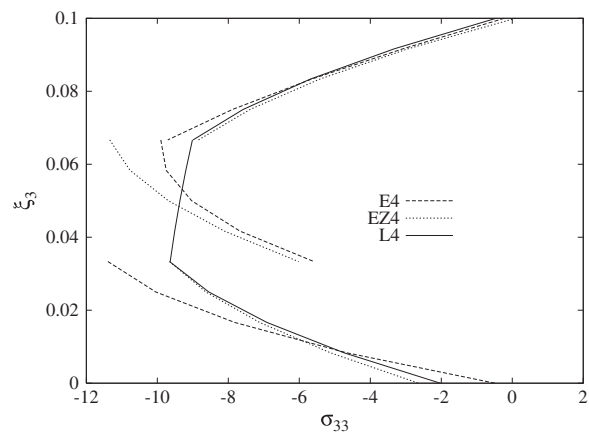
Figure 11. Varadan and Bhaskar cylinder. Distribution of transverse shear stress $\bar{\sigma}_{13}$ along the thickness. Lamination ($90°/0°/90°$). Thickness ratio $R/h = 100$.

Figure 12. Varadan and Bhaskar cylinder. Distribution of transverse normal stress $\bar{\sigma}_{33}$ along the thickness. Lamination ($90°/0°/90°$). Thickness ratio $R/h = 100$.

is able to fulfill the continuity conditions of transverse stresses at the interfaces between layers, whereas the FSDT model gives a completely wrong result (Figure 11), even if the shell is very thin ($R/h = 100$). In particular, Figures 10 ($R/h = 500$) and 12 ($R/h = 100$) show that the introduction of Murakami's zigzag function improves the solution in respect to a simple ESL model, but it is not enough to correctly describe the distribution of the normal stress in the composite structures because the interlaminar continuity conditions are not satisfied. For this reason, the results in terms of displacements are also better when a LW model is used. One can note that in Figure 12, the normal stress σ_{33} is not equal to the load applied at the inner surface $(\hat{p}_3^+ = 1)$. This is due to the FEM approximation that makes difficult to match the exact value of σ_{33} also in $\xi_3 = 0$ (Table X). Anyway, this result can be considered satisfying in respect to the approximated solutions provided in the literature.

8. CONCLUSION

This paper has presented the static analysis of cylindrical composite structures by means of a shell finite element based on the CUF by Carrera [81, 82]. The results have been provided in terms of displacement, in-plane stresses, and transverse stresses for various thickness ratios from very thick to very thin shells. The performances of the shell element have been tested, and the different theories (classical and refined) contained in the CUF have been compared. The conclusions that can be drawn are the following:

1. The shell element is completely locking free, even when the shell is very thin, and the results converge to the exact solution by increasing the order of expansion of the displacements in the thickness direction;
2. When the shell is very thick, the LW models work better than ZZ ones, and these last ones work better than ESL models;
3. The classical models, such as CLT and FSDT, completely fail in the analysis of thick shells;
4. The use of LW models is mandatory for both thick and thin shells if one needs to accurately describe the distribution of transverse stresses in the thickness and to satisfy the interlaminar continuity conditions.

Future works could be devoted to consider the dynamic analysis of composite structures. Moreover, an isoparametric shell finite based on the CUF will be implemented in order to study structures with arbitrary geometry and to perform nonlinear analysis.

APPENDIX A: EXPLICIT FORM OF STIFFNESS FUNDAMENTAL NUCLEUS

The stiffness fundamental nucleus $\boldsymbol{K}^{\tau s i j}$ is as follows:

$$\boldsymbol{K}^{\tau s i j} = \begin{bmatrix} K_{11} & K_{12} & K_{13} \\ K_{21} & K_{22} & K_{23} \\ K_{31} & K_{32} & K_{33} \end{bmatrix}. \tag{A.1}$$

The subscript k, indicating the layer, is here omitted for brevity reasons. The elements of the nucleus are the following:

$$\begin{aligned}
K_{11} = {} & C_{55} N_{i_{m1}} \lhd N_{m1} N_{n1} \rhd_\Omega N_{j_{n1}} \lhd HF_{\tau,3} F_{s,3} \rhd_A + \\
& C_{11} N_{i,1_{m1}} \lhd N_{m1} N_{n1} \rhd_\Omega N_{j,1_{n1}} \lhd HF_\tau F_s \rhd_A + \\
& C_{16} N_{i,2_{m3}} \lhd N_{m3} N_{n1} \rhd_\Omega N_{j,1_{n1}} \lhd HF_\tau F_s \rhd_A + \\
& C_{16} N_{i,1_{m1}} \lhd N_{m1} N_{n3} \rhd_\Omega N_{j,2_{n3}} \lhd HF_\tau F_s \rhd_A + \\
& C_{66} N_{i,2_{m3}} \lhd N_{m3} N_{n3} \rhd_\Omega N_{j,2_{n3}} \lhd HF_\tau F_s \rhd_A
\end{aligned}$$

$$K_{12} = -C_{45}\frac{1}{R}N_{i_{m1}} \lhd N_{m1}N_{n2} \rhd_\Omega N_{j_{n2}} \lhd HF_{\tau,3}F_s \rhd_A +$$
$$C_{45}N_{i_{m1}} \lhd N_{m1}N_{n2} \rhd_\Omega N_{j_{n2}} \lhd H^2F_{\tau,3}F_{s,3} \rhd_A +$$
$$C_{12}N_{i,1_{m1}} \lhd N_{m1}N_{n2} \rhd_\Omega N_{j,2_{n2}} \lhd H^2F_\tau F_s \rhd_A +$$
$$C_{16}N_{i,1_{m1}} \lhd N_{m1}N_{n3} \rhd_\Omega N_{j,1_{n3}} \lhd H^2F_\tau F_s \rhd_A +$$
$$C_{26}N_{i,2_{m3}} \lhd N_{m3}N_{n2} \rhd_\Omega N_{j,2_{n2}} \lhd H^2F_\tau F_s \rhd_A +$$
$$C_{66}N_{i,2_{m3}} \lhd N_{m3}N_{n3} \rhd_\Omega N_{j,1_{n3}} \lhd H^2F_\tau F_s \rhd_A$$

$$K_{13} = C_{13}N_{i,1_{m1}} \lhd N_{m1}N_j \rhd_\Omega \lhd HF_\tau F_{s,3} \rhd_A +$$
$$C_{36}N_{i,2_{m3}} \lhd N_{m3}N_j \rhd_\Omega \lhd HF_\tau F_{s,3} \rhd_A +$$
$$C_{12}\frac{1}{R}N_{i,1_{m1}} \lhd N_{m1}N_{n2} \rhd_\Omega N_{j_{n2}} \lhd H^2F_\tau F_s \rhd_A +$$
$$C_{26}\frac{1}{R}N_{i,2_{m3}} \lhd N_{m3}N_{n2} \rhd_\Omega N_{j_{n2}} \lhd H^2F_\tau F_s \rhd_A +$$
$$C_{55}N_{i_{m1}} \lhd N_{m1}N_{n1} \rhd_\Omega N_{j,1_{n1}} \lhd HF_{\tau,3}F_s \rhd_A +$$
$$C_{45}N_{i_{m1}} \lhd N_{m1}N_{n2} \rhd_\Omega N_{j,2_{n2}} \lhd HF_{\tau,3}F_s \rhd_A$$

$$K_{21} = -C_{45}\frac{1}{R}N_{i_{m2}} \lhd N_{m2}N_{n1} \rhd_\Omega N_{j_{n1}} \lhd HF_\tau F_{s,3} \rhd_A +$$
$$C_{45}N_{i_{m2}} \lhd N_{m2}N_{n1} \rhd_\Omega N_{j_{n1}} \lhd H^2F_{\tau,3}F_{s,3} \rhd_A +$$
$$C_{12}N_{i,2_{m2}} \lhd N_{m2}N_{n1} \rhd_\Omega N_{j,1_{n1}} \lhd H^2F_\tau F_s \rhd_A +$$
$$C_{16}N_{i,1_{m3}} \lhd N_{m3}N_{n1} \rhd_\Omega N_{j,1_{n1}} \lhd H^2F_\tau F_s \rhd_A +$$
$$C_{26}N_{i,2_{m2}} \lhd N_{m2}N_{n3} \rhd_\Omega N_{j,2_{n3}} \lhd H^2F_\tau F_s \rhd_A +$$
$$C_{66}N_{i,1_{m3}} \lhd N_{m3}N_{n3} \rhd_\Omega N_{j,2_{n3}} \lhd H^2F_\tau F_s \rhd_A$$

$$K_{22} = C_{22}N_{i,2_{m2}} \lhd N_{m2}N_{n2} \rhd_\Omega N_{j,2_{n2}} \lhd H^3F_\tau F_s \rhd_A +$$
$$C_{26}N_{i,2_{m2}} \lhd N_{m2}N_{n3} \rhd_\Omega N_{j,1_{n3}} \lhd H^3F_\tau F_s \rhd_A$$
$$C_{26}N_{i,1_{m3}} \lhd N_{m3}N_{n2} \rhd_\Omega N_{j,2_{n2}} \lhd H^3F_\tau F_s \rhd_A +$$
$$C_{66}N_{i,1_{m3}} \lhd N_{m3}N_{n3} \rhd_\Omega N_{j,1_{n3}} \lhd H^3F_\tau F_s \rhd_A +$$
$$C_{44}\frac{1}{R^2}N_{i_{m2}} \lhd N_{m2}N_{n2} \rhd_\Omega N_{j_{n2}} \lhd HF_\tau F_s \rhd_A -$$
$$C_{44}\frac{1}{R}N_{i_{m2}} \lhd N_{m2}N_{n2} \rhd_\Omega N_{j_{n2}} \lhd H^2F_\tau F_{s,3} \rhd_A -$$
$$C_{44}\frac{1}{R}N_{i_{m2}} \lhd N_{m2}N_{n2} \rhd_\Omega N_{j_{n2}} \lhd H^2F_{\tau,3}F_s \rhd_A +$$
$$C_{44}N_{i_{m2}} \lhd N_{m2}N_{n2} \rhd_\Omega N_{j_{n2}} \lhd H^3F_{\tau,3}F_{s,3} \rhd_A$$

$$K_{23} = C_{22}\frac{1}{R}N_{i,2_{m2}} \lhd N_{m2}N_{n2} \rhd_\Omega N_{j_{n2}} \lhd H^3F_\tau F_s \rhd_A +$$
$$C_{23}N_{i,2_{m2}} \lhd N_{m2}N_j \rhd_\Omega \lhd H^2F_\tau F_{s,3} \rhd_A +$$
$$C_{26}\frac{1}{R}N_{i,1_{m3}} \lhd N_{m3}N_{n2} \rhd_\Omega N_{j_{n2}} \lhd H^3F_\tau F_s \rhd_A +$$
$$C_{36}N_{i,1_{m3}} \lhd N_{m3}N_j \rhd_\Omega \lhd H^2F_\tau F_{s,3} \rhd_A -$$

$$C_{45}\frac{1}{R}N_{i_{m2}} \triangleleft N_{m2}N_{n1} \triangleright_\Omega N_{j,1_{n1}} \triangleleft HF_\tau F_s \triangleright_A -$$

$$C_{44}\frac{1}{R}N_{i_{m2}} \triangleleft N_{m2}N_{n2} \triangleright_\Omega N_{j,2_{n2}} \triangleleft HF_\tau F_s \triangleright_A +$$

$$C_{45}N_{i_{m2}} \triangleleft N_{m2}N_{n1} \triangleright_\Omega N_{j,1_{n1}} \triangleleft H^2 F_{\tau,3} F_s \triangleright_A +$$

$$C_{44}N_{i_{m2}} \triangleleft N_{m2}N_{n2} \triangleright_\Omega N_{j,2_{n2}} \triangleleft H^2 F_{\tau,3} F_s \triangleright_A$$

$$K_{31} = C_{55}N_{i,1_{m1}} \triangleleft N_{m1}N_{n1} \triangleright_\Omega N_{j_{n1}} \triangleleft HF_\tau F_{s,3} \triangleright_A +$$

$$C_{45}N_{i,2_{m2}} \triangleleft N_{m2}N_{n1} \triangleright_\Omega N_{j_{n1}} \triangleleft HF_\tau F_{s,3} \triangleright_A +$$

$$C_{12}\frac{1}{R}N_{i_{m2}} \triangleleft N_{m2}N_{n1} \triangleright_\Omega N_{j,1_{n1}} \triangleleft H^2 F_\tau F_s \triangleright_A +$$

$$C_{13} \triangleleft N_i N_{n1} \triangleright_\Omega N_{j,1_{n1}} \triangleleft HF_{\tau,3} F_s \triangleright_A +$$

$$C_{26}\frac{1}{R}N_{i_{m2}} \triangleleft N_{m2}N_{n3} \triangleright_\Omega N_{j,2_{n3}} \triangleleft H^2 F_\tau F_s \triangleright_A +$$

$$C_{36} \triangleleft N_i N_{n3} \triangleright_\Omega N_{j,2_{n3}} \triangleleft HF_{\tau,3} F_s \triangleright_A$$

$$K_{32} = C_{22}\frac{1}{R}N_{i_{m2}} \triangleleft N_{m2}N_{n2} \triangleright_\Omega N_{j,2_{n2}} \triangleleft H^3 F_\tau F_s \triangleright_A +$$

$$C_{23} \triangleleft N_i N_{n2} \triangleright_\Omega N_{j,2_{n2}} \triangleleft H^2 F_{\tau,3} F_s \triangleright_A +$$

$$C_{26}\frac{1}{R}N_{i_{m2}} \triangleleft N_{m2}N_{n3} \triangleright_\Omega N_{j,1_{n3}} \triangleleft H^3 F_\tau F_s \triangleright_A +$$

$$C_{36} \triangleleft N_i N_{n3} \triangleright_\Omega N_{j,1_{n3}} \triangleleft H^2 F_{\tau,3} F_s \triangleright_A -$$

$$C_{45}\frac{1}{R}N_{i,1_{m1}} \triangleleft N_{m1}N_{n2} \triangleright_\Omega N_{j_{n2}} \triangleleft HF_\tau F_s \triangleright_A -$$

$$C_{44}\frac{1}{R}N_{i,2_{m2}} \triangleleft N_{m2}N_{n2} \triangleright_\Omega N_{j_{n2}} \triangleleft HF_\tau F_s \triangleright_A +$$

$$C_{45}N_{i,1_{m1}} \triangleleft N_{m1}N_{n2} \triangleright_\Omega N_{j_{n2}} \triangleleft H^2 F_\tau F_{s,3} \triangleright_A +$$

$$C_{44}N_{i,2_{m2}} \triangleleft N_{m2}N_{n2} \triangleright_\Omega N_{j_{n2}} \triangleleft H^2 F_\tau F_s \triangleright_A$$

$$K_{33} = C_{22}\frac{1}{R^2}N_{i_{m2}} \triangleleft N_{m2}N_{n2} \triangleright_\Omega N_{j_{n2}} \triangleleft H^3 F_\tau F_s \triangleright_A +$$

$$C_{23}\frac{1}{R}N_{i_{m2}} \triangleleft N_{m2}N_j \triangleright_\Omega \triangleleft H^2 F_\tau F_{s,3} \triangleright_A +$$

$$C_{23}\frac{1}{R} \triangleleft N_i N_{n2} \triangleright_\Omega N_{j_{n2}} \triangleleft H^2 F_{\tau,3} F_s \triangleright_A +$$

$$C_{33} \triangleleft N_i N_j \triangleright_\Omega \triangleleft HF_{\tau,3} F_{s,3} \triangleright_A +$$

$$C_{55}N_{i,1_{m1}} \triangleleft N_{m1}N_{n1} \triangleright_\Omega N_{j,1_{n1}} \triangleleft HF_\tau F_s \triangleright_A +$$

$$C_{45}N_{i,2_{m2}} \triangleleft N_{m2}N_{n1} \triangleright_\Omega N_{j,1_{n1}} \triangleleft HF_\tau F_s \triangleright_A +$$

$$C_{45}N_{i,1_{m1}} \triangleleft N_{m1}N_{n2} \triangleright_\Omega N_{j,2_{n2}} \triangleleft HF_\tau F_s \triangleright_A +$$

$$C_{44}N_{i,2_{m2}} \triangleleft N_{m2}N_{n2} \triangleright_\Omega N_{j,2_{n2}} \triangleleft HF_\tau F_s \triangleright_A$$

where the following symbols are introduced:

$$\triangleleft (.....) \triangleright_\Omega = \int_{\Omega_k} (.....) \mathrm{d}\Omega_k \quad \text{and} \quad \triangleleft (.....) \triangleright_A = \int_{\xi_3^k} (.....) \mathrm{d}\xi_3^k.$$

Both the integrals in the domain and along the thickness are numerically solved using the Gaussian quadrature rule. In particular, the number of Gauss points taken along the thickness is 6, which ensures the exact solution of the integrals even when an order of expansion $N = 4$ is considered.

REFERENCES

1. Noor AK, Rarig PL. Three-dimensional solutions of laminated cylinders. *Computer Methods in Applied Mechanics and Engineering* 1974; **3**:319–334.
2. Malik M. Differential quadrature method in computational mechanics: new development and applications. *Ph.D Dissertation*, University of Oklahoma, Oklahoma, 1994.
3. Malik M, Bert CW. Differential quadrature analysis of free vibration of symmetric cross-ply laminates with shear deformation and rotatory inertia. *Shock and Vibration* 1995; **2**:321–338.
4. Liew KM, Han B, Xiao M. Differential quadrature method for thick symmetric cross-ply laminates with first-order shear flexibility. *International Journal of Solids and Structures* 1996; **33**:2647–2658.
5. Davi G. Stress field in general composite laminates. *American Institute of Aeronautics and Astronautics Journal* 1996; **34**:2604–2608.
6. Ferreira AJM, Roque CC, Carrera E, Cinefra M. Analysis of thick isotropic and cross-ply laminated plates by radial basis functions and unified formulation. *Journal of Sound and Vibration* 2011; **330**:771–787.
7. Ferreira AJM, Roque CC, Carrera E, Cinefra M, Polit O. Analysis of laminated shells by a sinusoidal shear deformation theory and radial basis functions collocation, accounting for through-the-thickness deformations. *Composites Part B* 2011; **42**:1276–1284.
8. Ferreira AJM, Roque CC, Carrera E, Cinefra M. Analysis of laminated doubly-curved shells by a layer-wise theory and radial basis functions collocation, accounting for through-the-thickness deformations. *Computational Mechanics* 2011; **48**(1):13–25.
9. Reddy JN, Robbins DH. Theories and computational models for composite laminates. *Applied Mechanics Review* 1994; **47**:147–165.
10. Varadan TK, Bhaskar K. Review of different theories for the analysis of composites. *Journal of Aerospace Society of India* 1997; **49**:202–208.
11. Carrera E. Developments, ideas and evaluations based upon Reissner's mixed variational theorem in the modeling of multilayered plates and shells. *Applied Mechanics Review* 2001; **54**:301–329.
12. MacNeal RH. Perspective on finite elements for shell analysis. *Finite Elements in Analysis and Design* 1998; **30**:175–186.
13. Argyris JH. Matrix displacement analysis of plates and shells, Prolegomena to a general theory, part I. *Ingeniur-Archiv* 1966; **35**:102–142.
14. Sabir AB, Lock AC. The application of finite elements to the large deflection geometrically non-linear behaviour of cylindrical shells. In *Variational Methods in Engineering 2*, Brebbia CA, Tottenham H (eds). Southampton University Press: Southampton, England, 1972; 7/66–7/75.
15. Wempner GA, Oden JT, Kross DA. Finite element analysis of thin shells. *Journal of Engineering Mechanics ASCE 94* 1968; **94**:1273–1294.
16. Abel JF, Popov EP. Static and dynamic finite element analysis of sandwich structures. *Proceedings of the Second Conference of Matrix Methods in Structural Mechanics*, Vol. AFFSL-TR-68-150, Wright-Patterson Air Force Base, Ohio, USA, 1968; 213–245.
17. Monforton GR, Schmidt LA. Finite element analyses of sandwich plates and cylindrical shells with laminated faces. *Proceedings of the Second Conference of Matrix Methods in Structural Mechanics*, Vol. AFFSL-TR-68-150, Wright-Patterson Air Force Base, Ohio, USA, 1968; 573–308.
18. Pryor CW, Barker RM. A finite element analysis including transverse shear effect for applications to laminated plates. *American Institute of Aeronautics and Astronautics Journal* 1971; **9**:912–917.
19. Noor AK. Finite element analysis of anisotropic plates. *American Institute of Aeronautics and Astronautics Journal* 1972; **11**:289–307.
20. Hughes TJR, Tezduyar T. Finite elements based upon Mindlin plate theory with particular reference to the four-node isoparametric element. *Journal of Applied Mechanics* 1981; **48**:587–596.
21. Panda SC, Natarajan R. Finite element analysis of laminated composites plates. *International Journal for Numerical Methods in Engineering* 1979; **14**:69–79.
22. Parisch H. A critical survey of the 9-node degenerated shell element with special emphasis on thin shell application and reduced integration. *Computer Methods in Applied Mechanics and Engineering* 1979; **20**:323–350.
23. Ferreira AJM, Barbosa JT, Marques AT, De Sà JC. Non-linear analysis of sandwich shells: the effect of core plasticity. *Computers & Structures* 2000; **76**:337–346.
24. Zienkiewicz OC, Taylor RL, Too JM. Reduced intergration technique in general analysis of plates and shells. *International Journal for Numerical Methods in Engineering* 1973; **3**:275–290.
25. Chinosi C, Lovadina C. Remarks on partial selective reduced integration method for Reissner–Mindlin plate problem. *Computers & Structures* 1999; **73**:73–78.
26. Pugh EDL, Hintonand E, Zienkiewicz OC. A study of quadrilater plate bending elements with reduced integration. *International Journal for Numerical Methods in Engineering* 1978; **12**:1059–1079.
27. Hughes TJR, Cohen M, Horaun M. Reduced and selective integration techniques in the finite element methods. *Nuclear Engineering and Design* 1978; **46**:203–222.
28. Malkus DS, Hughes TJR. Mixed finite element methods—reduced and selective integration techniques: a unified concepts. *Computer Methods in Applied Mechanics and Engineering* 1978; **15**:63–81.

29. Chinosi C, Della Croce L, Scapolla T. Solving thin Naghdi shells with special finite elements. *Mathematical Modeling & Scientific Computing* 1997; **8**:231–240.
30. Chinosi C, Della C, L, Scapolla T. Hierarchic finite elements for thin Naghdi shell model. *International Journal of Solids and Structures* 1998; **35**(16):1863–1880.
31. Naghdi PM. The theory of shells and plates. In *Handbuch der Physic*, Vol. 4. Springer: Berlin, 1972; 425–640.
32. Bathe KJ, Dvorkin EN. A four node plate bending element based on Mindlin/Reissner plate theory and mixed interpolation. *International Journal for Numerical Methods in Engineering* 1985; **21**:367–383.
33. Bathe KJ, Brezzi F, Cho SW. The MITC7 and MITC9 plate elements. *Computers and Structures* 1989; **32**:797–814.
34. Bathe KJ, Brezzi F, Fortin M. Mixed interpolated elements for Reissner–Mindlin plates. *International Journal for Numerical Methods in Engineering* 1989; **28**:1787–1801.
35. Huang NC, Hinton E. A nine node Lagrangian Mindlin plate element with enhanced shear interpolation. *Engineering Computations* 1984; **1**:369–379.
36. Auricchio F, Sacco L. A mixed-enhanced finite elements for the analysis of laminated composites. *International Journal for Numerical Methods in Engineering* 1999; **44**:1481–1504.
37. Brank B, Carrera E. A family of shear-deformable shell finite elements for composite structures. *Computer & Structures* 2000; **76**:287–297.
38. Arnold DN, Brezzi F. Locking-free finite element methods for shells. *Mathematics of Computation* 1997; **66**(217):1–14.
39. Büchter N, Ramm E. 3D-extension of non-linear shell equations based on the enhanced assumed strain concept. In *Computational Methods in Applied Sciences*, Hirsch C (ed.). Elsevier: San Diego, CA, USA, 1992; 55–62.
40. Bischoff M, Ramm E. Shear-deformable shell elements for large strains and rotations. *International Journal for Numerical Methods in Engineering* 1997; **40**:4427–4449.
41. Bischoff M, Ramm E. On the physical significance of higher-order kinematic and static variables in a three-dimensional shell formulation. *International Journal of Solids and Structures* 2000; **37**:6933–6960.
42. Bletzinger KU, Bischoff M, Ramm E. A unified approach for shear-locking-free triangular and rectangular shell finite elements. *Computers & Structures* 2000; **75**:321–334.
43. Braun M, Bischoff M, Ramm E. Non linear shell formulations for complete three-dimensional constitutive laws including composites and laminates. *Computational Mechanics* 1994; **15**:1–18.
44. Simo JC, Rafai S. A class of mixed assumed strain methods and the method of incompatible modes. *International Journal for Numerical Methods in Engineering* 1990; **29**:1595–1638.
45. Kant T, Owen DRJ, Zienkiewicz OC. Refined higher order C^0 plate bending element. *Computer & Structures* 1982; **15**:177–183.
46. Kant T, Kommineni JR. Large amplitude free vibration analysis of cross-ply composite and sandwich laminates with a refined theory and C0 finite elements. *Computer & Structures* 1989; **50**:123–134.
47. Dau F, Polit O, Touratier M. C^1 plate and shell finite elements for geometrically nonlinear analysis of multilayered structures. *Computer & Structures* 2006; **84**:1264–1274.
48. Dau F, Polit O, Touratier M. An efficient C^1 finite element with continuity requirements for multilayered/sandwich shell structures. *Computer & Structures* 2004; **82**:1889–1899.
49. Polit O, Touratier M. A multilayered/sandwich triangular finite element applied to linear and non-linear analyses. *Composite Structures* 2002; **58**:121–128.
50. Polit O, Touratier M. High-order triangular sandwich plate finite element for linear and non-linear analyses. *Computational Methods in Applied Mechanics and Engineering* 2000; **185**:305–324.
51. Polit O, Touratier M. A new laminated triangular finite element assuring interface continuity for displacements and stresses. *Composite Structures* 1997; **38**(1-4):37–44.
52. Tessler A. A higher-order plate theory with ideal finite element suitability. *Computer Methods in Applied Mechanics and Engineerings* 1991; **85**:183–205.
53. Reddy JN. *Mechanics of Laminated Composite Plates and Shells*, Theory and Analysis. CRC Press: New York, USA, 1997.
54. Palazotto AN, Dennis ST. *Nonlinear Analysis of Shell Structures*. AIAA Educational Series: Washington, DC, 1992.
55. Disciuva M, Cicorello A, Dalle Mura E. A class of multilayered anisotropic plate elements including the effects of transverse shear deformabilty. *Proceedings of AIDAA Conference*, Torino, 1985; 877–892.
56. Bekou A, Touratier M. A rectangular finite element for analysis composite multilayerd shallow shells in static, vibration and buckling. *International Journal for Numerical Methods in Engineering* 1993; **36**:627–653.
57. Reissner E. On a certain mixed variational theorem and on laminated elastic shell theory. *Proceedings of the Euromech-Colloquium* 1986; **219**:17–27.
58. Rao KM, Meyer-Piening HR. Analysis of thick laminated anisotropic composites plates by the finite element method. *Composite Structures* 1990; **15**:185–213.
59. Carrera E. A class of two-dimensional theories for anisotropic multilayered plates analysis. *Accademia delle Scienze di Torino, Memorie Scienze Fisiche* 1995; **19–20**:1–39.
60. Murakami H. Laminated composite plate theory with improved in-plane responses. *Journal of Applied Mechanics* 1986; **53**:661–666.
61. Brank B, Carrera E. Multilayered shell finite element with interlaminar continuous shear stresses: a refinement of the Reissner–Mindlin formulation. *International Journal for Numerical Methods in Engineering* 2000; **48**:843–874.

62. Noor AK, Burton WS. Assessment of computational models for multi-layered composite shells. *Applied Mechanics Review* 1990; **43**:67–97.
63. Reddy JN. An evaluation of equivalent single layer and layer-wise theories of composite laminates. *Composite Structures* 1993; **25**:21–35.
64. Mawenya AS, Davies JD. Finite element bending analysis of multilayer plates. *International Journal for Numerical Methods in Engineering* 1974; **8**:215–225.
65. Pinsky PM, Kim KO. A multi-director formulation for nonlinear elastic–viscoelastic layered shells. *Computers & Structures* 1986; **24**:901–913.
66. Chaudhuri RA, Seide P. An approximate method for prediction of transverse shear stresses in a laminated shell. *International Journal of Solids and Structures* 1987; **23**:1145–1161.
67. Rammerstorfer FG, Dorninger K, Starlinger A. Composite and sandwich shells. In *Nonlinear Analysis of Shells by Finite Elements*, Rammerstorfer FG (ed.). Springer-Verlag: Vienna, 1992; 131–194.
68. Carrera E. Theories and finite elements for multilayered anisotropic composite plates and shells. *Archives of Computational Methods in Engineering* 2002; **9**:87–140.
69. Carrera E. Theories and finite elements for multilayered plates and shells: a unified compact formulation with numerical assessment and benchmarking. *Archives of Computational Methods in Engineering* 2003; **10**(3):215–296.
70. Bathe KJ, Lee PS, Hiller JF. Towards improving the MITC9 shell element. *Computers and Structures* 2003; **81**:477–489.
71. Chinosi C, Della Croce L. Mixed-interpolated elements for thin shell. *Communications in Numerical Methods in Engineering* 1998; **14**:1155–1170.
72. Huang NC. Membrane locking and assumed strain shell elements. *Computners and Structures* 1987; **27**(5):671–677.
73. Panasz P, Wisniewski K. Nine-node shell elements with 6 dofs/node based on two-level approximations. Part I Theory and linear tests. *Finite Elements in Analysis and Design* 2008; **44**:784–796.
74. Koiter WT. On the foundations of the linear theory of thin elastic shell. *Proc. Kon. Nederl. Akad. Wetensch.* 1970; **73**:169–195.
75. Ciarlet PG, Gratie L. Another approach to linear shell theory and a new proof of Korn's inequality on a surface. *C. R. Acad. Sci. Paris, Ser. I* 2005; **340**:471–478.
76. Chapelle D, Bathe KJ. *The Finite Element Analysis of Shells—Fundamentals*. Springer: Berlin, 2003.
77. Bathe K-J, Dvorkin E. A formulation of general shell elements—the use of mixed interpolation of tensorial components. *International Journal for Numerical Methods in Engineering* 1986; **22**:697–722.
78. Bucalem ML, Bathe K-J. Higher-order MITC general shell elements. *International Journal for Numerical Methods in Engineering* 1993; **36**:3729–3754.
79. Ren JG. Exact solutions for laminated cylindrical shells in cylindrical bending. *Composites Sciences and Technology* 1987; **29**:169–187.
80. Varadan TK, Bhaskar K. Bending of laminated orthotropic cylindrical shells—an elasticity approach. *Composite Structures* 1991; **17**:141–156.
81. Carrera E. Multilayered shell theories accounting for layerwise mixed description, Part 2: numerical evaluations. *AIAA Journal* 1999; **37**(9):1117–1124.
82. Carrera E. Multilayered shell theories accounting for layerwise mixed description, Part 1: governing equations. *AIAA Journal* 1999; **37**(9):1107–1116.